Journal of ELECTRONIC MATERIALS, Vol. 50, No. 4, 2021
https://doi.org/10.1007/s11664-020-08712-8

ORIGINAL RESEARCH ARTICLE

Numerical Simulation of CZTSe Based Solar Cells Using Different Back Surface Field Layers: Improvement and Comparison

RKIA EL OTMANI,[1] AHMED EL MANOUNI ,[1,3,4] and ABDELMAJID AL MAGGOUSSI[2]

1.—Laboratoire LPAMM, Département de Physique, Faculté des Sciences et Techniques, Université Hassan II, BP 145 Mohammedia, Morocco. 2.—IMED-LabGEMO, Faculté des Sciences et Techniques, Université Cadi Ayyad, BP 549, 40000 Marrakech, Morocco. 3.—e-mail: elmanouni123@gmail.com. 4.—e-mail: ahmed.elmanouni@fstm.ac.ma

This work reports on a numerical modeling of $Cu_2ZnSnSe_4$ (CZTSe) thin film based solar cells using Solar Cell Capacitance Simulator (SCAPS). First, a conventional CZTSe/CdS/ZnO solar cell structure has been proposed and optimized. The optimal output parameters (power conversion efficiency PCE = 24.50%, short circuit current density J_{sc} = 47.732 mA/cm^2, fill factor FF = 80.478% and open circuit voltage V_{oc} = 0.639 V) have been obtained for ZnO, CdS and CZTSe layer thicknesses closed to 0.02 μm, 0.02 μm and 1.5 μm, respectively. Next, to improve on the conventional solar cell performance, three cell structures with different highly P-doped materials as back surface field (BSF) layers, such as P^+-CZTSe, P^+-Cu_2O and P^+-CZTS, have been proposed and optimized. In comparison to the conventional cell, devices with BSF layer have shown improvements of all the photovoltaic parameters. The CZTS/CZTSe/CdS/ZnO device has provided the highest performance (PCE = 25.83%, J_{sc} = 51.04 mA/cm^2, FF = 78.14% and V_{oc} = 0.646 V) for ZnO, CdS, CZTSe and P^+-CZTS thicknesses closed to 0.02 μm, 0.02 μm, 1.5 μm and 0.4 μm, respectively. Additionally, the generation rate is no affected by the BSF layer; however, the recombination rate has decreased in the bulk and back surface of the CZTSe absorber. Finally, the insertion of the BSF layer has caused an increase of external quantum efficiency (EQE) up to 94.5% and a slight red shift of absorption in the long-wavelength region near the band edge.

Key words: CZTSe, kesterite, numerical simulation, solar cells, back surface field, SCAPS-1D

INTRODUCTION

In order to meet the growing energy demands, several research teams in the world focus their efforts on the synthesis of solar cells based on thin absorber materials which must provide solar energy production with higher efficiency and low cost. During the last decade, research works on the photovoltaic field have focused on the copper-indium-selenide (CIS), copper-indium-gallium-selenide (CIGS) and cadmium telluride (CdTe) thin films. Solar cells based on these materials have provided record power conversion efficiencies (PCE) of 21.5% for CdTe[1] and 21.7% for CIGS[2]. Despite this performance, the development of these materials has been interrupted due, in one hand, to the toxicity of cadmium (Cd) and its membership in heavy metal family and, in the other hand, to the lack of telluride (Te) and the high cost of indium (In) and gallium (Ga)[3]. Therefore, researchers have explored other ways using eco-friendly materials with earth-abundant elements[4,5].

(Received August 28, 2020; accepted December 17, 2020; published online January 15, 2021)

Copper-zinc-selenium quaternary $Cu_2ZnSnSe_4$ (CZTSe) have emerged as a potential photovoltaic material to substitute CIGS absorber materials in thin film solar cells[6,7]. It is considered to be the most promising semiconductor due to its excellent properties, such as its large natural abundance in the earth crust (Cu: 25 ppm, Zn: 71 ppm, Sn: 5.5 ppm), its appropriate direct optical band gap ranging 0.9–1.4 eV[8] and its high optical absorption coefficient exceeding 10^4 cm^{-1}[8,9]. However, solar cells based on CZTSe thin film suffer from low experimental power conversion efficiency (PCE) in comparison to solar cells based on CdTe and CIGS thin films, since the highest measured PCE is 12.6%[5], which is still far from the widely accepted Shockley-Queisser limit value of 28%[10]. The low efficiency has been mainly attributed to a large deficit in the open circuit voltage (V_{oc}) relative to the band gap of the absorber layer[11]. The low V_{oc} could be due to recombination losses at the poorly optimized buffer/absorber and/or to absorber/back interfaces and to the high series resistance (R_s) especially for thicker active layers[11,12]. To boost high CZTSe solar cells efficiency improvements must be performed by minimizing current and voltage losses. Numerical simulation methods can guide us in this direction to achieve a valuable upstream work.

One well-known technique to improve PCE is the insertion of high P-doping material at the back surface of the absorber layer thereby forming a back surface field (BSF). Indeed, it has been reported that solar cells without BSF layer have produced lower performance than solar devices with BSF contact due to loss of photogenerated carriers by back recombination process[13]. Applying a BSF layer at the back side of the absorber could improve the carrier collection by an additional drift field induced by the electrons and the current density is enhanced by the inhibition of recombination at the back contact side. Additionally, the BSF material should have a low lattice mismatch in comparison to the absorber layer and an energy band structure able to transfer photocarriers to electrode[11,14].

CZTSe is a quaternary *p*-type semiconductor due to the presence of native defects, such as copper vacancy V_{Cu}, copper on zinc antisite Cu_{Zn}, zinc on copper antisite Zn_{Cu} and zinc on tin antisite Zn_{Sn} defects[15–18] depending on the growth technique. Various methods have been used to prepare CZTSe thin films including sputtering, evaporation, hydrazine-based chemical approach, and electrodeposition techniques[5,19–21]. The CSTSe alloy exhibits the kesterite type structure[22,23] and a direct band gap energy between 0.9 eV and 1.4 eV at room temperature depending on the stoichiometry of the compound[8,24].

In this work, the photovoltaic behaviour of CZTSe kesterite thin film based solar cells with and without a BSF layer has been modelled and analysed using the Solar Cell Capacitance Simulator (SCAPS-1D) program. As a comparison basis, a conventional solar structure ZnO/CdS/CZTSe is modelled and optimized. Next, different highly P-doped materials have been inserted as a BSF contact and their effect on the photovoltaic performance, such as the band diagram energy, the PCE, the external quantum efficiency (EQE), and generation (Ge) and recombination (Re) rates was examined deeply. Finally, a comparative study on the performance of the proposed devices with and without BSF material has been carried out.

METHODOLOGY AND SIMULATION CONDITIONS

Numerical Simulation SCAPS

SCAPS is a one-dimensional solar cell simulation program developed with LabWindows/CVI of National Instruments at the University of Gent[25]. It was developed for simulating the electrical characteristics of thin-film heterojunction solar cells with CIGS and CdTe thin film absorbers. However, several modifications in this software have improved its capabilities to work with crystalline solar cells (silicon, Si, and gallium arsenic, GaAs, family) and amorphous cells (a-Si and micromorphous Si)[25]. The need for numerical modeling of thin film polycrystalline solar cells is relevant as the absorber/buffer interface involving hetero-junctions is more complex in nature[26]. SCAPS allows alternating current (AC) and direct current (DC) electrical measurements which can be calculated in the dark and under light illumination and also at different temperatures, including the open circuit voltage (V_{oc}), short circuit current density (J_{sc}), fill factor (FF%), power conversion efficiency (PCE%), external quantum efficiency (EQE%), capacitance frequency spectroscopy *C(f)*, capacitance voltage spectroscopy *C(V)*, generation and recombination profiles, and carrier current densities[26].

SCAPS software provides electrical characteristics of thin-film heterojunction solar cells by solving the three well-known basic semiconductor equations (1-3) governing the steady state conditions: Poisson's equation (Eq. 1) and electron and hole continuity equations (Eqs 2 and 3).

$$-\ \text{Poisson equation}: \left(\frac{\partial^2\psi}{\partial x^2}\right) = -\frac{q}{\varepsilon_0\varepsilon_r}\left(p - n + N_D^+ - N_A^- + \frac{\rho_{\text{def}}}{q}\right) \tag{1}$$

$$-\ \text{Continuity equations}: \frac{\partial n}{\partial t} = -\frac{1}{q}\frac{\partial J_n}{\partial x} + G - R_n \tag{2}$$

$$\frac{\partial p}{\partial t} = -\frac{1}{q}\frac{\partial J_p}{\partial x} + G - R_p \tag{3}$$

The charge carrier transport described by the drift and diffusion is expressed by the following equations:

$$J_n = -qn\mu_n \frac{\partial \psi}{\partial x} + qD_n \frac{\partial n}{\partial x} \tag{4}$$

$$J_p = -qp\mu_p \frac{\partial \psi}{\partial x} - qD_p \frac{\partial p}{\partial x} \tag{5}$$

The general current equation is

$$J = J_0\left(\exp\left(\frac{qV}{AKT}\right) - 1\right) - J_{ph} \tag{6}$$

where ψ is the electrostatic potential, $\varepsilon_0/\varepsilon_r$ is the permittivity of free space/the relative permittivity of the absorber, q is the magnitude of charge of the electron, n and p are the free carrier concentrations, N_D^+ and N_A^- are the density of ionised donors and acceptors, ρ_{def} is the charge density of defects, G is the carrier generation rate, R_n/R_p is the carrier recombination rate of electrons/holes, $J_n/\ J_p$ is the current density of electrons/holes, K is the Boltzmann constant, T is the temperature, J_{ph} is the photoelectric current density and J_0 is the reverse saturation current density given by:

$$J_0 = Aq\left[\frac{D_p P_{n_0}}{L_p} + \frac{D_n n_{p_0}}{L_n}\right] \tag{7}$$

where D_n/D_p is the diffusion constant of electrons/holes, L_n and L_p are the diffusion length of each carrier type, p_{no} and n_{p0} are the majority carrier concentrations on the p and n side. A is the diode ideality factor depending on the current transport, A = 1 for injection/diffusion mechanism and A = 2 for recombination mechanism.

The Poisson and the continuity equations, with appropriate boundary conditions at the interfaces and contacts, lead to a system of coupled differential equations in (Ψ, n, p) or (Ψ, E_{Fn}, E_{Fp}). Solving this system of equations provides the electrical parameters of the solar cell, such as the V_{oc}, J_{sc}, FF, and PCE[27].

Design of CZTSe-Based Solar Cells

Two types of solar cells, shown in Fig. 1, have been proposed and studied: the first type is a conventional device formed of three input layers ($Cu_2ZnSnSe$ absorber, CdS buffer and ZnO window layers) and its substrate structure is Pt/$Cu_2ZnSnSe_4$/CdS/ZnO/Al and the second type consists of solar cells with BSF material and their substrate structures are Pt/P^+-Cu_2O/$Cu_2ZnSnSe_4$/CdS/ZnO/Al, Pt/P^+-$Cu_2ZnSnSe_4$/$Cu_2ZnSnSe_4$/CdS/ZnO/Al and Pt/P^+-Cu_2ZnSnS_4/$Cu_2ZnSnSe_4$/CdS/ZnO/Al. For the conventional cell, the p-$Cu_2ZnSnSe_4$ film is the active layer with an acceptor concentration of 5×10^{16} cm^{-3} and a variable thickness in the range of 0.1–4 μm, the n-CdS layer is the buffer layer with a donor concentration of 1×10^{18} cm^{-3} and a thickness ranging from 0.01 to 0.1 μm, the ZnO material is the window layer with a donor concentration of 1×10^{18} cm^{-3} and thickness variable from 0.01 to 0.1 μm. For solar cells with BSF layer, three high P-doped materials (P^+-Cu_2O, P^+-$Cu_2ZnSnSe_4$, P^+-Cu_2ZnSnS_4) were inserted at the back surface of the CZTSe absorber layer in order to make the back contact more ohmic and, especially, to improve the efficiency. For each BSF material, the acceptor carrier concentration was set to 1×10^{21} cm^{-3} and the thickness was varied in the range of 0.1–1 μm.

Main Input Parameters

The numerical resolution of the basic semiconductor equations via the SCAPS software program requires knowledge of electrical and physical properties of all involved layers in the proposed devices as well as electrical and optical parameters, deep

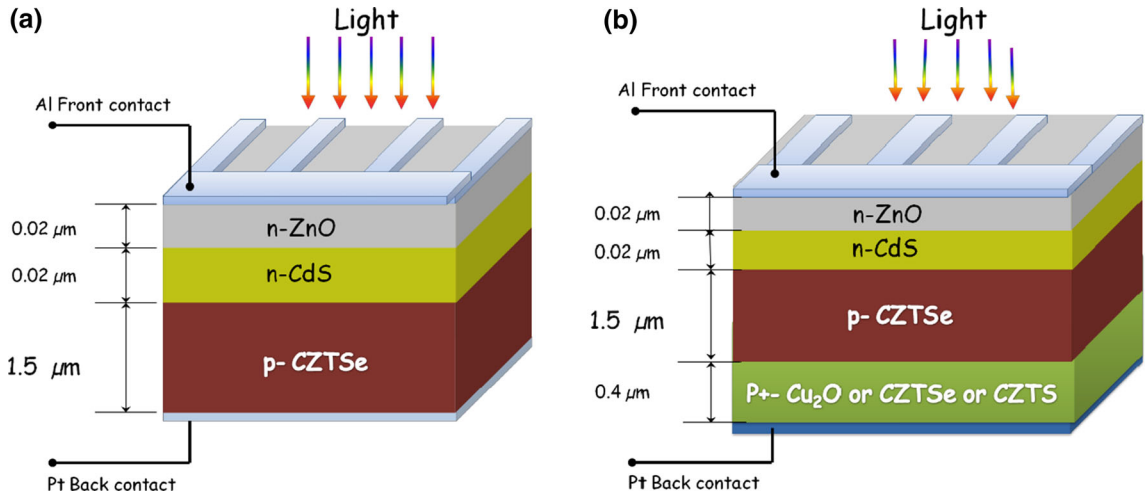

Fig. 1. Schematic diagram of the optimized CZTSe based thin film solar cells. (a) Conventional device (b) Device with BSF layer.

bulk defects and interface defect recombination (radiative and non-radiative recombination).

Front and Back Contacts and Surfaces

The back and front contacts have significant effects on the performance of solar cells, especially the back contact which acts as an optical reflector to the photons that are not absorbed in the active medium, and as a metallic contact layer to transport drive out the photo-generated carriers[28]. In addition, the back contact material should have a higher work function than the neighboring light-absorbing semiconductor layer to realize ohmic contact[29]. In our simulation, the front and back contacts are in aluminum and platinum, respectively, and both are ohmic, since the following condition $\varphi_{Al} \prec (E_g + \chi)_{CdS} / \varphi_{Pt} \succ (E_g + \chi)_{CZTSe}$ is verified for the front contact/rear contact, where $\phi_{\mathrm{Al}} / \phi_{\mathrm{pt}}$ is the work function of aluminum/platinum and $(E_{\mathrm{g}} + \chi)_{\mathrm{CZTSe}} / (E_{\mathrm{g}} + \chi)_{\mathrm{CdS}}$ is the sum of the band gap energy and electron affinity of p-CZTSe/ n-CdS material. Additionally, the front surface reflectivity R_{f} and the back surface reflectivity R_{b} were set to 0.05 and 0.8, respectively.

Physical and Electrical Material Parameters for Layers

In order to simulate photovoltaic characteristics of the proposed solar cells several parameters relative to all involved layers have to be inputted

Table I. Basic parameters used in simulation of CZTSe based solar cells.

Contact parameters	**Front contact (Al)**		**Back contact (Pt)**
Work function Φ (eV)	4.45[30]		5.4[31]
Surface recombination velocity of electrons Se (cm/s)	10^7 [SCAPS]		10^7 [SCAPS]
Surface recombination velocity of holes Sh (cm/s)	10^7 [SCAPS]		10^7 [SCAPS]
Reflectivity R_{f}	0.05		0.8
Physical layer properties	n–ZnO[32]	—CdS[32]	p-CZTSe
Thickness (μm)	0.01-0.1 variable	0.01-0.1 variable	0.1–4 variable
Band gap (eV)	3.37	2.43	1.02[20]
Electron affinity (eV)	4.45	4	4.28[33]
Dielectric constant	9.00	9.35	13.6[33,34]
CB effective density of state for electron (cm^{-3}) Nc	2.95×10^{18}	1.76×10^{18}	9.15×10^{17} *calculated*
VB effective density of states (cm^{-3}) Nv	1.14×10^{19}	1.47×10^{19}	4.54×10^{18} *calculated*
Electron thermal velocity (cm/s)	2.38×10^7	2.83×10^7	3.6×10^7 *calculated*
Hole thermal velocity (cm/s)	1.52×10^7	1.39×10^7	2.06×10^7 *calculated*
Electron mobility (cm^2/Vs) at 300K	100	100	100[33,34]
Hole mobility (cm^2/Vs) at 300K	25	25	12.5[33,34]
Shallow uniform donor density n (cm^{-3})	1.0×10^{18}	1.0×10^{18}	0
Shallow uniform acceptor density p (cm^{-3})	0	0	5×10^{16} optimized by SCAPS
Defect layer properties			
Energy defect level respect to valence band edge E_{V} (eV)	1.65	1.2	0.052[15] 0.449[15]
Shallow donor density N_{D} (cm^{-3})	1.73×10^{18}	1.77×10^{18}	0
Shallow acceptor density N_{A} (cm^{-3})	0	0	1.1×10^{15} 2.2×10^{15} [SCAPS]
Thermal capture cross section of electron (cm^{-2})	1.0×10^{-15}	1.0×10^{-15}	1.1×10^{-15} [SCAPS]
Thermal capture cross section of hole (cm^{-2})	1.0×10^{-15}	1.0×10^{-15}	1.0×10^{-15} [SCAPS]
Optical capture cross section of electron (cm^{-2})	1.0×10^{-12}	1.0×10^{-13}	1.0×10^{-13} [SCAPS]
Optical capture cross section of hole (cm^{-2})	1.0×10^{-12}	1.0×10^{-13}	1.0×10^{-13} [SCAPS]

in the SCAPS simulator program. These parameters include band gap energy (E_g), electron affinity (χ), dielectric permittivity (ε), conduction band density of states (N_C), valence band density of states (N_V), electron thermal velocity ($V_{th,n}$), hole thermal velocity ($V_{th,p}$), electron mobility (μ_n), hole mobility (μ_p), donor density (N_D), acceptor density (N_A), as seen in Table I. For our simulation, the input parameters were either calculated or extracted from the literature or imported from the database of SCAPS program. Also, all calculations have been carried out at temperature of 300 K and under standard illumination AM1.5.

Defect States

The SCAPS software can integrate two defect types for each layer: shallow and deep defects. The first is defined as one shallow level completely ionized and it does not contribute to the recombination process. The second can be represented by more than three deep levels governed by the Shockley-Read-Hall model[35]. Deep levels contribute to the recombination process in different interfaces and within layers and the charge of each level is defined by its occupation and its conductivity type (donor or acceptor or neutral). The energy distribution of deep levels can be modelled either by a single level, uniform band, Gaussian distribution or exponential repartition. The input parameters relative to defect states are the capture cross sections for electron and hole, σ_e and σ_p, defect distribution, N_{def} (E) and total density of deep levels, N_t. In this simulation, CdS and ZnO layer defects have been assumed as neutral deep levels with Gaussian distributions, whereas two uniform acceptor single levels localised at 0.449 eV and 0.052 eV in respect to valence band edge E_V have been introduced for CZTSe absorber layer. These acceptor defects are due to the copper vacancy V_{Cu} and copper antisite tin Cu_{sn} defects, respectively[15,20].

Furthermore, more input parameters relative to defects for each BSF material must be introduced. In the case of the P^+-Cu_2O layer, two uniform acceptor single levels localised at 0.21 eV and 0.5 eV with respect to valence band edge E_V are considered due to Cu di-vacancy and Cu vacancy defects, respectively[36]. For P^+-CZTSe and P^+-CZTS BSF layers the input parameters of defects are similar to those used in P-CZTSe absorber material as depicted in Table II.

RESULTS AND DISCUSSION

The main objective of this work is to provide the optimal design and performance of solar cells based on CZTSe thin films. To achieve this objective, two types of CZTSe solar cells (with and without BSF contact) have been simulated and optimized and their photovoltaic parameters have been calculated and analyzed.

Table II. Added input parameters for the simulation of BSF layers.

	P^+-CZTSe	P^+-CZTS	P^+-Cu_2O
Physical properties of BSF layer			
Thickness (μm)	0.1–1 variable	0.1–1varaible	0.1–1 variable
Gap energy (eV)	1.02[20]	1.50[37,38]	2[39,40]
Electron affinity (eV)	4.28[33,34]	4.5[33]	3.2[40]
Dielectric constant	13.6[33,34]	10[33]	7.11[41]
CB effective density of state for electron (cm^{-3}) Nc	9.15×10^{17} Calculated	2.07×10^{18} Calculated	2.46×10^{19} Calculated
VB effective density of states (cm^{-3}) Nv	4.54×10^{18} Calculated	1.59×10^{19} Calculated	1.1×10^{19} Calculated
Electron thermal velocity (cm/s)	3.6×10^{7} Calculated	2.68×10^{7} Calculated	1.17×10^{7} Calculated
Hole thermal velocity (cm/s)	2.06×10^{17} Calculated	1.39×10^{7} Calculated	1.53×10^{7} Calculated
Electron mobility (cm^2/Vs) at 300K	100[33,34]	100[33]	200[42]
Hole mobility (cm^2/Vs) at 300K	12.5[33,34]	25[33]	67[42]
Shallow uniform donor density n (cm^{-3})	–	–	–
Shallow uniform acceptor density p (cm^{-3})	1.0×10^{21}	1.0×10^{21}	1.0×10^{21}
Defect layer properties			
Defect energy respect to valence band edge	0.449[15] 0.052[15]	0.449[15] 0.052[15]	0.5[36] 0.21[36]
Density of carriers in defect (cm^{-3})	1.1×10^{17} 2.2×10^{17} [SCAPS]	1.1×10^{17} 2.2×10^{17} [SCAPS]	2.3×10^{16} 6.1×10^{16} [SCAPS]
Optical capture cross section of electron (cm^{-2})	10^{-15} [SCAPS]	10^{-15} [SCAPS]	10^{-15} [SCAPS]
Optical capture cross section of electron (cm^{-2})	10^{-15} [SCAPS]	10^{-15} [SCAPS]	10^{-15} [SCAPS]

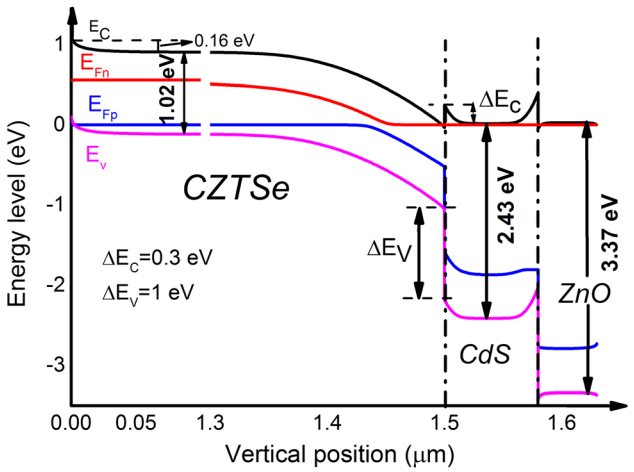

Fig 2. Energy band diagram of the conventional solar cell generated by the SCAPS software at the dark and zero bias voltage.

Analysis of the Conventional CZTSe Solar Cell

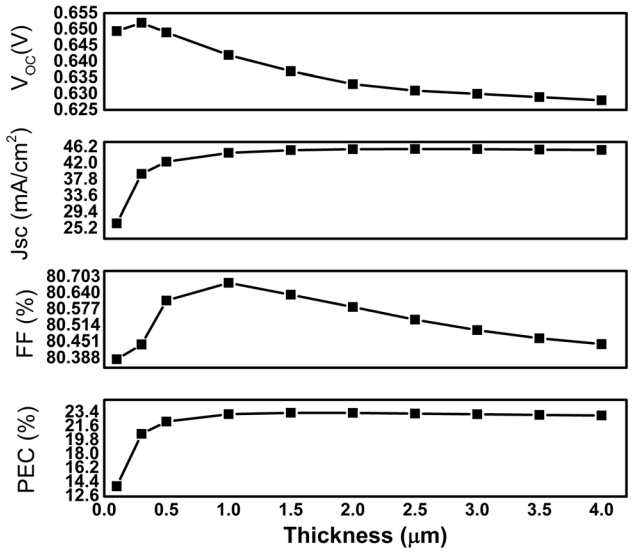

Fig 3. Photovoltaic characteristics for the conventional solar cell as a function of CZTSe absorber thickness.

Band Diagram

The band diagram of the CZTSe/CdS/ZnO conventional solar device is shown in Fig. 2. The diagram was generated by the SCAPS program in the dark at zero bias and the energy levels are given with respect to the Fermi level which is set to 0 eV. The diagram is plotted for CZTSe absorber, CdS buffer and ZnO window thicknesses closed to 1.5 μm, 0.08 μm, and 0.05 μm, respectively. It is observed that n-type and *p*-type regions and the associated valence band (VB) and conduction band (CB) edges and the interfaces and their positions are clearly shown in the figure. Also, we note the presence of reflecting barriers with heights of 0.16 eV and 0.24 eV for the Pt/CZTSe interface in conduction and valence bands, respectively, and a positive conduction band offset CBO (spike) of ΔE_c = 0.3 eV for the interface between CZTSe and CdS layers. The observed spike can be attributed to the difference between electron affinity of absorber and buffer layers and its value is less than values of 0.41–0.48 eV reported by Haight et al.[36] for a CZTSSe/CdS solar device. It should be noted that a small spike can be tunneled by photogenerated carriers and does not imply any major limitation on device performance by inhibiting the recombination process at CZTSe/CdS interface; however, a large spike can act as a barrier to electron flow from the absorber to the buffer, thus reducing the current density J_{sc}[43].

CZTSe Absorber Layer Optimization

Theoretically the minimum thickness required is approximately 2 μm for CZTSe layer to absorb 99% of the incident photons with energy greater than E_g. However, further numerical analysis must be done to reduce the thickness of CZTSe, CdS and ZnO layers aiming to conserve the material usage and cost of cell production. In this sense, the CZTSe absorber thickness has been varied from 0.1 to 4 μm to look for its optimal value. The obtained results are plotted in Fig. 3. It is observed that the PCE and J_{sc} are unaffected with a decrease of the CZTSe thickness from 4 to 1.5 μm; however, the V_{oc} and the FF have increased. Further reduction of CZTSe thickness ($<$ 1.5 μm) results in a slowly decrease of J_{sc} and PCE, whereas the V_{oc} and FF increased up to 0.3 μm and 1 μm, respectively. For CZTSe thickness less than 0.3 μm, J_{sc} has decreased sharply from 39.22 mA/cm^2 to 26.47 mA/cm^2 du to the shorter minority carrier diffusion length, but the FF and V_{oc} have been slightly affected because they have decreased from 80.44% to 80.38% and from 0.652 V to 0.649 V, respectively. As a combined effect, the PCE has decreased from its maximum value of 23.31%, when reducing CZTSe thickness below 1.5 μm. Above this value, the PCE has been slightly affected by a minor decreasing due both to the increasing of the resistivity and minor recombination losses occurring at different layer interfaces and at the back contact. According to this analysis, the optimal CZTSe thickness can be considered 1.5 μm and the corresponding output parameters are PCE = 23.31%, V_{oc} = 0.637 V, J_{sc} = 45.377 mA/cm^2 and FF = 80.633%.

Otherwise, in order to confirm the found optimal CZTSe thickness, we have calculated the total carrier generation rate Ge at various positions within the absorber of the conventional solar cell and plotted its variation in Fig. 4. From this figure, it is shown that the Ge value was 1.44×10^{22} cm^{-3} s^{-1} at the position near of the CZTSe/CdS interface and then it decreased drastically to 1.34×10^{20} cm^{-3} s^{-1} (by two orders of magnitude) within just 1.5 μm of CZTSe thickness before becoming constant for a CZTSe absorber thickness

up to 8 μm. This behavior confirms once more that the optimal CZTSe thickness is 1.5 μm, since the carrier generation is not affected by the increase of the thickness above 1.5 μm.

CZTSe Absorber, CdS Buffer and ZnO Window Optimization

It is well known that the window and the buffer layers affect the photovoltaic performance of solar cells. Thereby, to optimize the buffer CdS and ZnO window layers, the thickness of each material has been varied from 0.01 to 0.1 μm. The obtained results are presented in Fig. 5. One can remark that all output parameters have decreased with increasing ZnO thickness up to 0.1 μm, while the PCE and FF have increased with increasing CdS thickness up to 0.02 μm and then decreased. Nevertheless, the V_{oc} and J_{sc} have decreased with increasing CdS thickness up to 0.1 μm. From this analysis the optimal thickness for ZnO and CdS layers can be considered 0.02 μm. Furthermore, the optimization of ZnO and CdS layers has led to improvements of all photovoltaic parameters. The corresponding optimal values are summarized in Table III and are PCE = 24.50%, J_{sc} = 47.732 mA/cm^2, V_{oc} = 0.639 V and FF = 80.378% for ZnO, CdS and CZTSe thicknesses of 0.02 μm, 0.02 μm and 1.5 μm, respectively. Thus, the optimization of ZnO window and buffer CdS layers has lead to an enhancement of the PCE from 23.31 to 24.50%.

On the other hand, the conventional device (without BSF) has been modeled by the classical equivalent electrical circuit and its series resistance and shunt resistance have been calculated (see Table III). It is observed that the calculated series resistance is much lower than 1 Ω.cm^2 and the obtained series resistance and shunt resistance values are close to those reported in the literature[44,45]. Furthermore, the calculated series resistance value is one order of magnitude lower than that of CZTS devices, while the calculated shunt resistance value is close to that reported by H. Katagiri et al for CZTS thin film based solar cells (R_s = 4.25 Ω.cm^2 and R_{sh} = 370 Ω.cm^2)[46]. After the optimization of ZnO and CdS layers, the series resistance has slightly increased, while the shunt resistance has decreased significantly. This can be explained by the fact that when the layers become thin, the recombination process at CZTSe/CdS interface enhances.

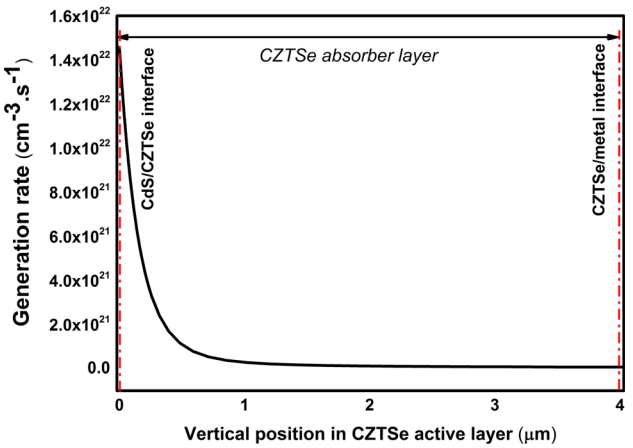

Fig 4. Total carrier generation rate for the conventional solar cell.

External Quantum Efficiency

Quantum efficiency is used as a tool for measuring the spectral response of the device. It provides detailed information about the absorption of photons and creation of carriers at different wavelength or photon energy levels. It is defined by the ratio of collected electrons from the device per incident photons at each wavelength:

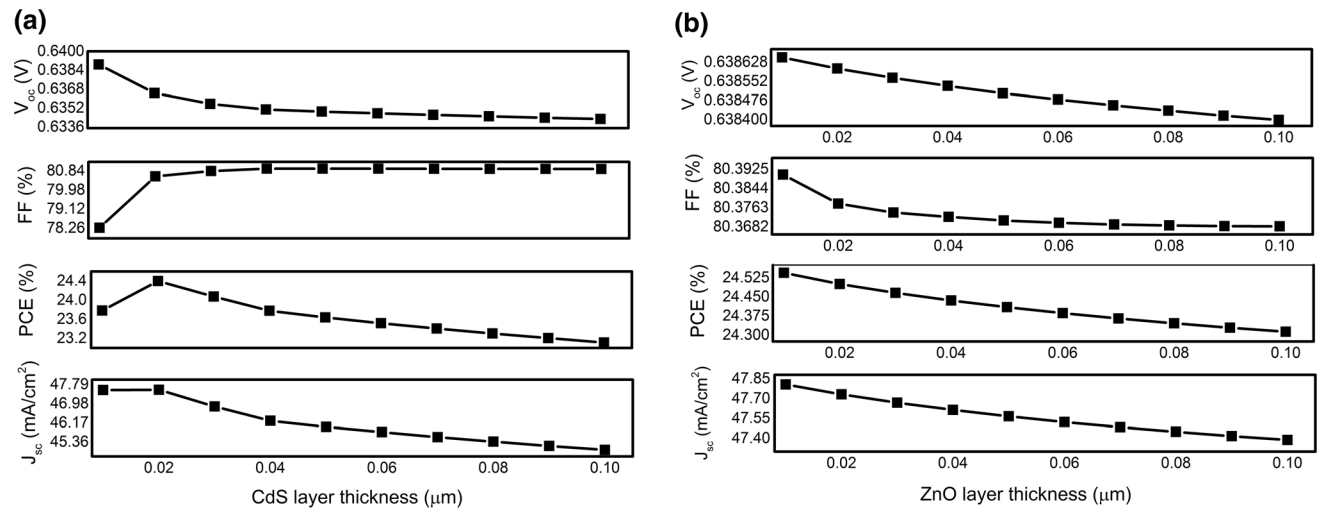

Fig 5. Photovoltaic performance of the conventional solar cell as function of (a) CdS and (b) ZnO layer thicknesses.

Table III. Optimal output parameters values for the conventional based solar cell.

Photovoltaic characteristics	PCE (%)	J_{sc} (mA/cm^2)	FF (%)	V_{oc} (V)	R_s (Ω cm^2)	R_{sh} (Ω cm^2)
CZTSe/CdS/ZnO	23.31	45.377	80.633	0.637	0.481	409.61
After optimization of ZnO and CdS layers	24.50	47.732	80.378	0.639	0.505	354.53

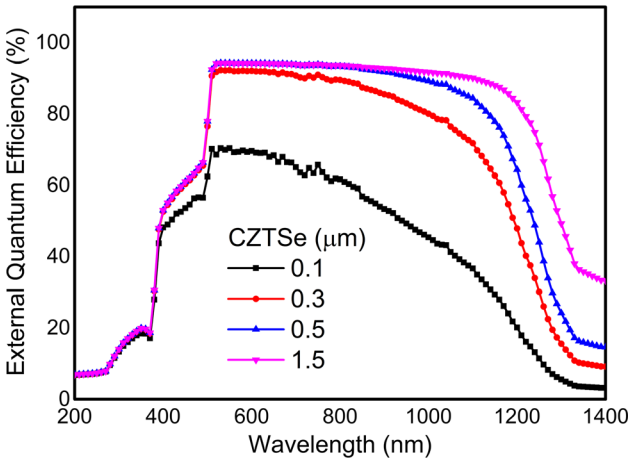

Fig 6. EQE spectra of the conventional CZTSe based solar cell.

$$\mathrm{EQE}(\lambda) = \frac{\mathrm{Numberofcollectedelectrons}}{\mathrm{Number\ of\ incident\ photons}} = \frac{I(\lambda)/q}{\varphi_{\mathrm{inc}}(\lambda)} \tag{8}$$

where the $I(\lambda)$ and $\phi_{\mathrm{inc}}(\lambda)$ are photogenerated current and photon flow, respectively.

Figure 6 shows the external quantum efficiency (EQE) of the conventional solar cell for various CZTSe thickness values ranging from 0.1 to 1.5 μm (for thickness greater than 1.5 μm, the curves are overlapped, not seen here). From the figure, the EQE spectra have shown a broad absorption feature in the wavelength range 200- 1400 nm and both EQE and the long-wavelength spectral response have decreased with decreasing the CZTSe thickness due to an insufficient absorption of photons which has occurred when the CZTSe layer has been thinner and/or to back recombination losses have become important. For the CZTSe absorber thickness greater than 1.5 μm, the EQE has remained constant and its maximum value is closed to 93% in the wavelength range 510–1100 nm. This result confirms once more that the optimal CZTSe thickness is 1.5 μm.

Analysis of CZTSe Solar Cells with BSF Layer

It has been reported that solar cells without BSF layer produce photovoltaic performance lower than solar devices with BSF contact due to the photogenerated carrier losses induced by the back recombination process[15]. Indeed, the BSF layer produces a back field which could repel the photogenerated carriers at the back surface of the absorber and, therefore, would increase the collected photocurrent. Additionally, the BSF material should have a low lattice mismatch in comparison with the absorber layer and an energy band structure able to transfer photocarriers to electrode[5].

In order to improve photovoltaic performance of the studied conventional CZTSe based solar cells, three highly P-doped appropriate materials has been carefully selected and inserted at the back surface of the CZTe active layer. The used BSF materials are P$^+$-Cu_2O, P$^+$-Cu_2ZnSnS_4 and P$^+$-$Cu_2ZnSnSe_4$ and their optical thicknesses have been varied and tuned to get the best possible PCE. A comparative study on photovoltaic characteristics of the conventional solar cell and the solar cells with BSF contact has beee performed.

Band Diagrams

Figure 7 shows the optimized band diagrams generated by SCAPS for the three proposed CZTSe solar devices with BSF contact at zero bias in the dark within the cells. The energy levels are shown in respect to the Fermi level, which is set to 0 eV in the band diagram. The substrate structures of the cells are P$^+$-Cu_2O/CZTSe/CdS/ZnO, P$^+$-CZTSe/CZTSe/CdS/ZnO and P$^+$-CZTS/CZTSe/CdS/ZnO. In comparison with the conventional solar cell, it is observed that the application of the BSF layer results in a positive band offsets (spikes) in the conduction and valence band at the back surface of the absorber for all the proposed BSF layers which would act as barriers for the photogenerated carriers. These barriers would reflect back the electrons from the conduction band interface of CZTSe-BSF towards the front contact and thus reduce the recombination losses of photogenerated carrier at the back interface.

Back Surface Field Layer Optimisation

In order to determine the BSF effect on the photovoltaic performance, numerical simulation of the main output parameters has been achieved. The absorber (CZTSe), window (ZnO) and buffer (CdS) thicknesses were set to their optimal values close to 1.5 μm, 0.02 μm and 0.02 μm and the BSF layer thickness was varied in the range of 0.1 to 2 μm for each BSF material. The obtained results are presented in Fig. 8. In comparison with the conventional cell (without BSF layer), all devices have shown an enhancement of PCE, J_{sc} and V_{oc}, whereas the FF has slightly decreased due probably

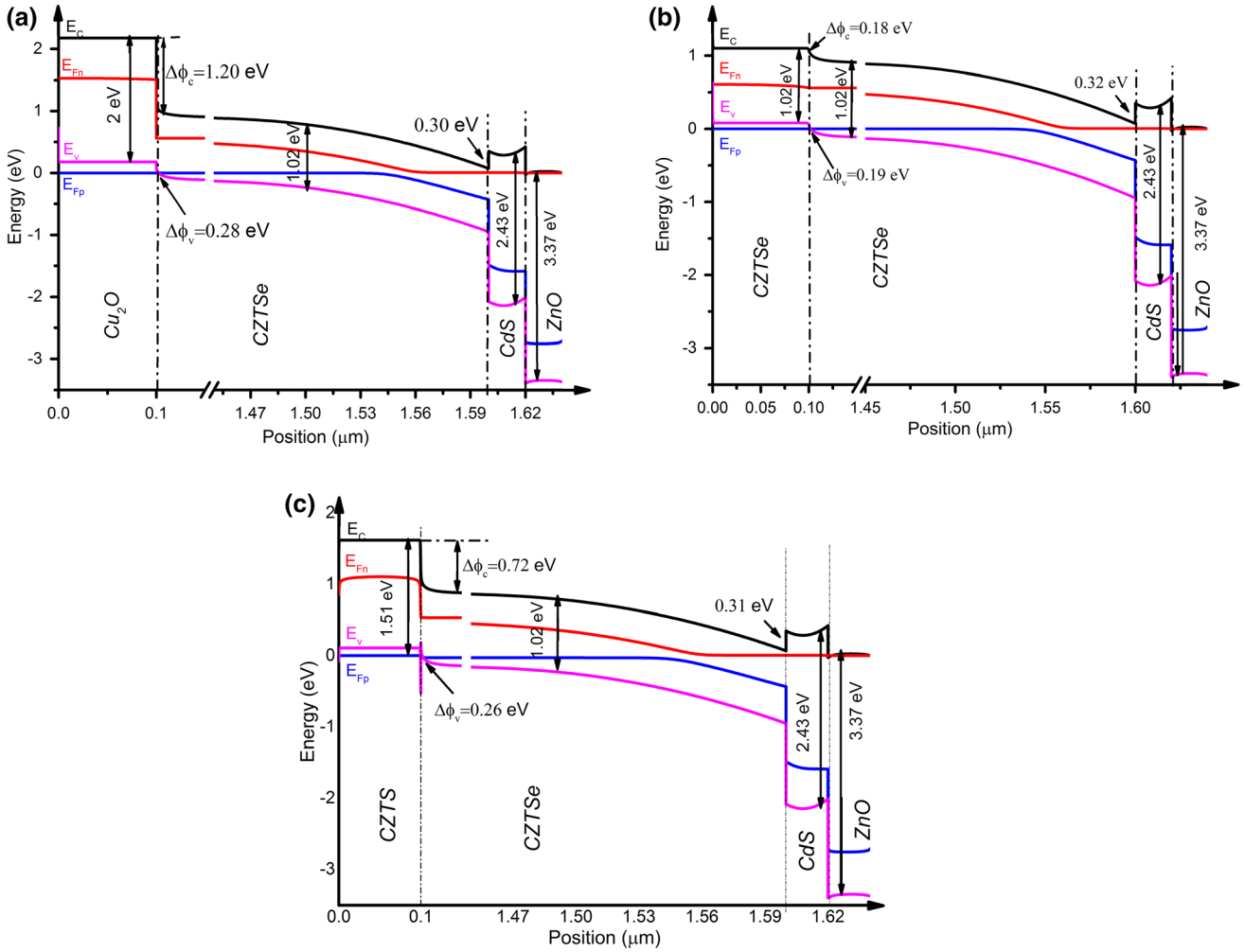

Fig 7. Optimized energy band diagrams of CZTSe solar devices at the dark and zero bias voltage with (a) P^+-Cu_2O, (b) P^+-CZTSe and (c) P^+-CZTS as BSF layers.

to an increase of series resistance. The analysis of the mean working parameters has showed that the insertion of a BSF layer has provided further improvement on the performance for all proposed devices and the solar cell with P^+-CZTS BSF layer has given the highest photovoltaic parameters. Figure 8 shows the variation of all output parameters as function of BSF layer thickness. From the figure, all output parameters have increased for P^+-CZTS layer thickness up to 0.4 μm, reached its maximum for 0.4 μm and then decreased for P^+-CZTS thickness varying from 0.4 to 2 μm, while they have decreased continually with increasing P^+-CZTSe and P^+-Cu_2O BSF layer thicknesses up to 2 μm, respectively. Based on this behavior, the optimal BSF layer thickness can be considered 0.4 μm for P^+-CZTS layer and 0.1 μm for both P^+-Cu_2O and P^+-CZTSe materials.

The photovoltaic characteristics of the optimized CZTSe thin film based solar cells with BSF layers are summarized in Table IV. In comparison to the conventional cell, the PCE has enhanced from 23.31 to 25.83%, the J_{sc} from 45.377 to 51.035 mA/cm^2 and V_{oc} from 0.637 to 0.646 V; however, the FF has decreased from 80.633 to 78.135%. The decrease in the fill factor (FF) is due to the parasitic resistance and the rather high reverse saturation current density J_0 of the devices[44]. In addition, the calculated series resistance R_s has slightly increased while the shunt resistance R_{sh} has decreased due probably to the increase of the electrical resistivity of the cells[46].

Effect of BSF Layer on Generation and Recombination Rates

In the literature, the reported efficiencies of kesterite solar cells are limited by interfacial recombination as the dominating recombination paths[11]. It has been demonstrated that sulfide-containing absorbers produce a conduction band cliff at the CZTS/CdS interface leading to interface recombination process[47]. This recombination process constitutes a major challenge to the front interface for

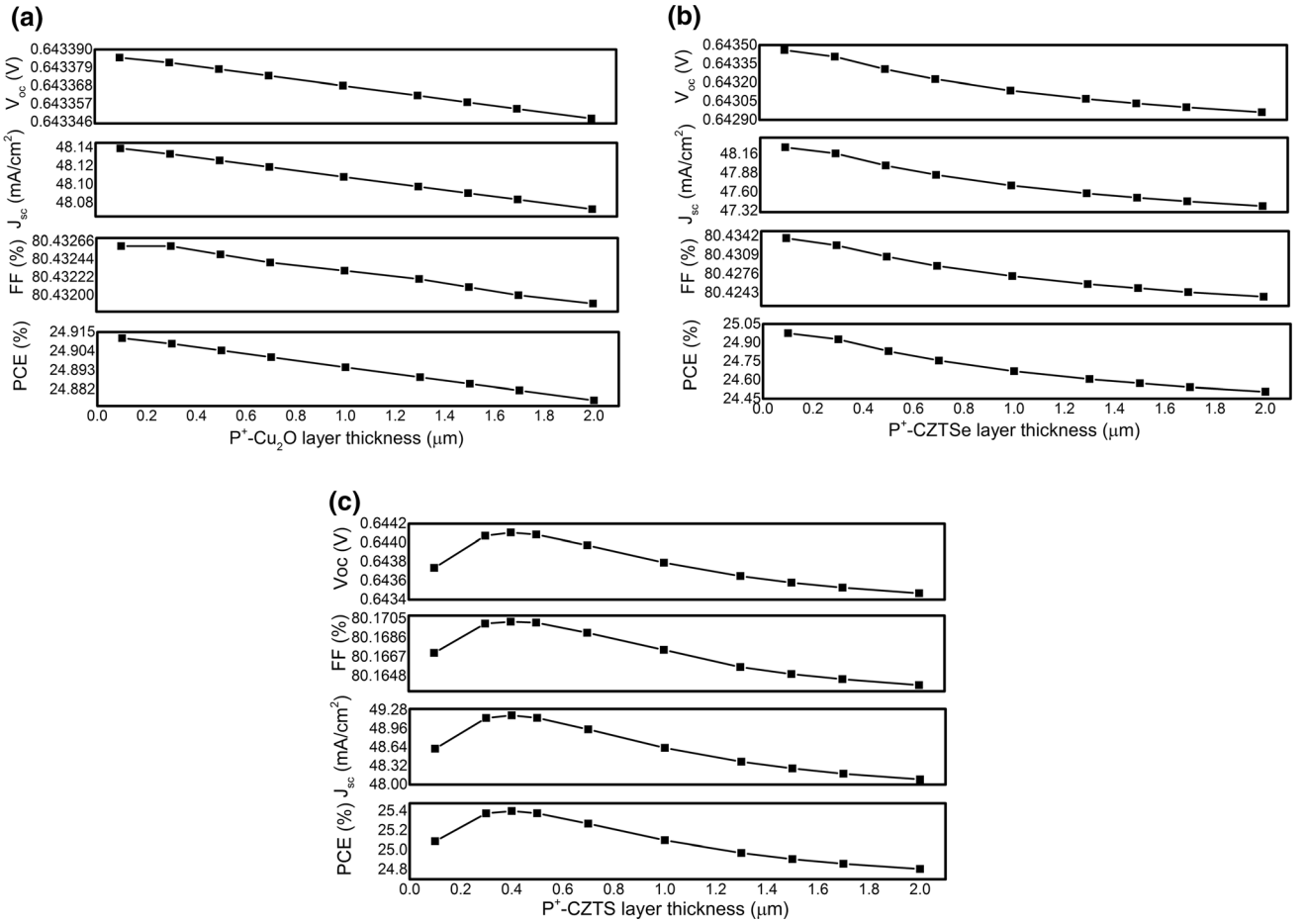

Fig 8. Photovoltaic performance of CZTSe solar cells as a function of BSF layer thickness, with (a) P$^+$-Cu_2O, (b) P$^+$-CZTSe and (c) P$^+$-CZTS as BSF layers.

Table IV. Optimal photovoltaic output parameters of CZTSe solar cells with BSF layer.

Solar cell	PCE (%)	J_{sc} (mA/cm^2)	FF (%)	V_{oc} (V)	R_s (Ω cm^2)	R_{sh} (Ω cm^2)
P$^+$-Cu_2O/CZTSe/CdS/ZnO	24.91	48.138	80.432	0.643	0.512	354.70
P$^+$-CZTSe/CZTSe/CdS/ZnO	24.97	48.257	80.433	0.643	0.506	350.95
P$^+$-CZTS/CZTSe/CdS/ZnO	25.83	51.036	78.135	0.646	0.541	316.80

improving the efficiency. On the other hand, the back contact plays a key role in the performance of kesterite solar devices. The back contact must contribute to produce an extra drift field for minority carriers, thus enhancing the carrier collection and inhibiting the bulk and surface recombination. According to our band diagram for the conventional CZTSe device, wherein a positive conduction band offset (spike) has been observed, it is expected that the carrier recombination does not occur at the interface between CdS buffer and CZTSe absorber. Furthermore, it is shown also that the presence of a barrier at the BSF/CZTSe interface for devices with BSF contact prevent back recombination from taking place. To confirm these, the generation (Ge) and recombination (Re) rates across the solar cell width for all studied structures are calculated and plotted in Fig. 9. Referring to the figure, one can see that the generation rate Ge is not affected by the BSF layer within the absorber film. Also, the recombination rate Re is closed to 8.4×10^{20} cm^{-3} s^{-1} in the window layer and then it has decreased sharply at the buffer/absorber and absorber/BSF interfaces. Furthermore, the insertion of a BSF layer has caused an important decrease of the Re within the CZTSe absorber in comparison to the conventional cell and a remarkable intense peak has appeared in the highly doped CSZTS BSF layer due to the high acceptor concentration of defects. These defects have acted as traps of photogenerated carriers and then enhanced the recombination process in the BSF material, as reported by Chen et al[15]. Based on

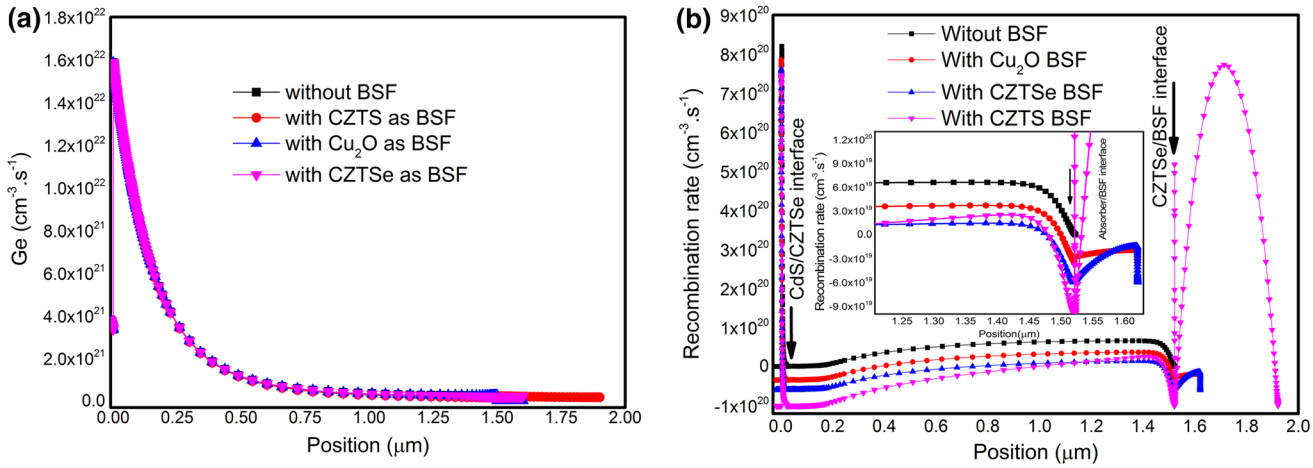

Fig 9. (a) Generation rate (Ge) and (b) recombination rate Re for CZTSe solar cells with and without BSF layer. The inset of graph 9b shows zoomed Re in 1.35-1.65 μm range.

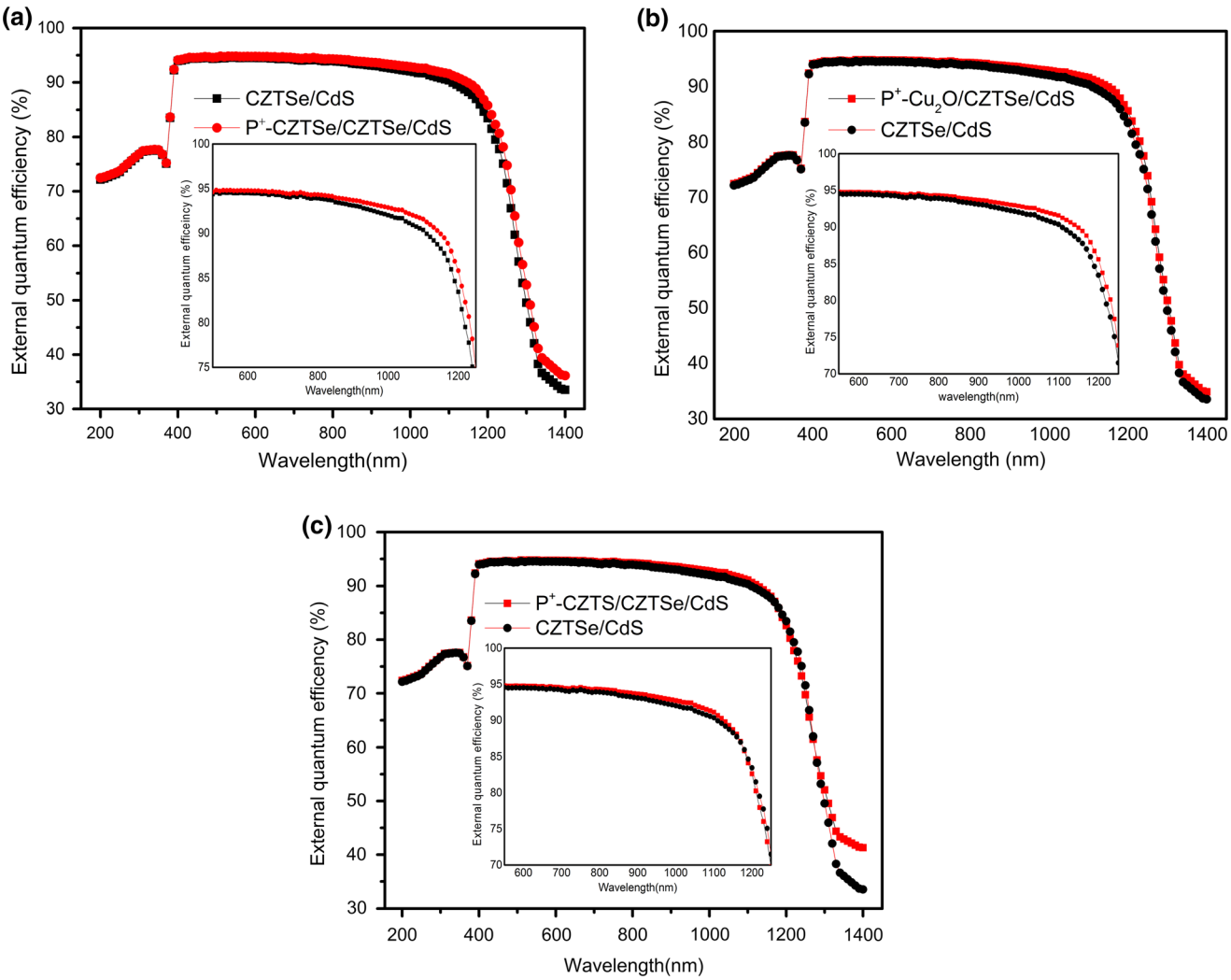

Fig 10. EQE of CZTSe solar cells as function of wavelength (Black: without BSF and red: with BSF; with (a) P^+-CZTSe, (b) P^+-Cu_2O and (c) P^+-CZTS as BBF material). The inset of each graph shows EQE zoomed curves in 600–1220 nm wavelength range (Color figure online).

band diagrams (Fig. 7) and recombination rate Re variation curves (Fig. 9), it seems that a combined effect of the observed positive conduction band offset (spike) at the CZTSe and CdS interface and the BSF layer has provided high efficiency.

Back Surface Field Layer Effect on External Quantum Efficiency

The external quantum efficiency (*EQE*) has been calculated for the optimized CZTSe based solar cells with and without BSF layer and plotted in Fig. 10. According to the figure, the insertion of the BSF layer has lead to an enhancement of the EQE with a maximum value of 94.5% achieved on device with the P^+-CZTS BSF layer and to a slight redshift of the absorption edge. The increase of EQE can be attributed to a weak recombination loss deep in the absorber layer and/or longer minority carrier diffusion length[15].

CONCLUSION

An effective method to increase the V_{oc} and the PCE of CZTSe thin film based solar cells by insertion of a back surface field (BSF) layer is reported in this work. Solar cells with and without BSF layer have been simulated using the SCAPS program. First, the influence of all involved layers on the CZTSe/CdS/ZnO conventional solar cell performance has been investigated and analyzed. The optimization of the CZTSe absorber layer, CdS buffer and ZnO window layers has led to an enhancement of the mean photovoltaic characteristics, except the V_{oc} which has slightly decreased, and provided the following output parameters: PCE = 24.50%, J_{sc} = 47. 732 mA/cm^2, FF = 80.478% and V_{oc} = 0.639 V for ZnO, CdS and CZTSe layer thicknesses closed to 0.02 μm, 0.02 μm and 1.5 μm, respectively. Next, to boost the conventional cell efficiency, three appropriated highly P-doped materials, such as P^+-CZTSe, P^+-Cu_2O and P^+-CZTS, have been applied and optimized. This results in an improvement of all photovoltaic characteristics. The highest output parameters (PCE = 25.83%, J_{sc} = 51.04 mA/cm^2, FF = 78.14% and V_{oc} = 0.646 V) have been achieved on the device with P^+-CZTS BSF material for ZnO, CdS, CZTSe and P^+-CZTS layer thicknesses closed to 0.02 μm, 0.02 μm, 1.5 μm and 0.4 μm, respectively. Additionally, the generation rate Ge has not been affected by the BSF layer within the absorber film, while the recombination rate has decreased sharply at the buffer/absorber and absorber/ BSF interfaces. Also, the insertion of BSF layer has caused a slight increase of EQE and a redshift of the absorption edge in the long-wavelength region. Finally, according to our results a combined effect of the observed positive conduction band offset (spike) at the CZTSe and CdS interface and the BSF layer has provided high efficiency.

ACKNOWLEDGEMENTS

The Authors acknowledge Mr. Marc Bargeman, from University of Gent, for providing SCAPS-1D software.

CONFLICT OF INTEREST

On behalf of all authors, the corresponding author states that there is no conflict of interest.

REFERENCES

1. M.A. Green, Y. Hishikawa, W. Warta, E.D. Dunlop, D.H. Levi, J.H. Ebinger, and A.W.H. Ho-Baillie, M.A. Green, Y. Hishikawa, W. Warta, E.D. Dunlop, D.H. Levi, J.H. Ebinger, and A.W.H. Ho-Baillie, *Prog. Photovolt. Res. Appl.*, 2017, **25**, p 668.
2. T. Kato, A. Handa, T. Yagioka, T. Matsuura, K. Yamamoto, S. Higashi, J.-L. Wu, K.F. Tai, H. Hiroi, T. Yoshiyama, T. Sakai, and H. Sugimoto, T. Kato, A. Handa, T. Yagioka, T. Matsuura, K. Yamamoto, S. Higashi, J.-L. Wu, K.F. Tai, H. Hiroi, T. Yoshiyama, T. Sakai, and H. Sugimoto, *IEEE J. Photovolt.*, 2017, **7**, p 1773.
3. Y. Kee-Jeong, S. Dae-Ho, S. Shi-Joon, S. Jun-Hyoung, K. Young-Ill, P. Si-Nae, J. Dong-Hwan, K. JungSik, H. Dae-Kue, J. Chan-Wook, N. Dahyun, C. Hyeonsik, K. Jin-Kyu, and K. Dae-Hwan, Y. Kee-Jeong, S. Dae-Ho, S. Shi-Joon, S. Jun-Hyoung, K. Young-Ill, P. Si-Nae, J. Dong-Hwan, K. JungSik, H. Dae-Kue, J. Chan-Wook, N. Dahyun, C. Hyeonsik, K. Jin-Kyu, and K. Dae-Hwan, *J. Mater. Chem. A*, 2016, **4**, p 10151.
4. W. Wang, M.T. Winkler, O. Gunawan, T. Gokmen, T.K. Todorov, Y. Zhu, and D.B. Mitzi, W. Wang, M.T. Winkler, O. Gunawan, T. Gokmen, T.K. Todorov, Y. Zhu, and D.B. Mitzi, *Adv. Energy Mater.*, 2014, **4**, p 1301465.
5. G. Brammertz, M. Buffière, S. Oueslati, H. ElAnzeery, K. Ben Messaoud, S. Sahayaraj, C. Köble, M. Meuris, and J. Poortmans, J. Appl. Phys. Lett. 103, 163904 (2013).
6. S. Siebentritt, and S. Schorr, S. Siebentritt, and S. Schorr, *Prog. Photovolt. Res. Appl.*, 2012, **20**, p 512.
7. D.B. Mitzi, O. Gunawan, T.K. Todorov, K. Wang, and S. Guha, D.B. Mitzi, O. Gunawan, T.K. Todorov, K. Wang, and S. Guha, *Sol. Energy Mater. Sol. Cells*, 2011, **95**, p 1421.
8. C. Guilin, W. Weihuang, C. Shuiyuan, W. Zhezhe, H. Zhigao, Z. Biyun, and K. Xiangkai, C. Guilin, W. Weihuang, C. Shuiyuan, W. Zhezhe, H. Zhigao, Z. Biyun, and K. Xiangkai, *J. Alloys Compd.*, 2017, **718**, p 236.
9. B. Schubert, B. Marsen, S. Cinque, T. Unold, R. Klenk, S. Schorr, and H.W. Schock, B. Schubert, B. Marsen, S. Cinque, T. Unold, R. Klenk, S. Schorr, and H.W. Schock, *Prog. Photovolt. Res. Appl.*, 2011, **19**, p 93.
10. D.B. Mitzi, O. Gunawan, T.K. Todorov, and D.A.R. Barkhouse, D.B. Mitzi, O. Gunawan, T.K. Todorov, and D.A.R. Barkhouse, *Phil. Trans. R. Soc. A*, 2013, **371**, p 20110432.
11. S. Bourdais, C. Chone, B. Delatouche, A. Jacob, G. Larramona, C. Moisan, A. Lafond, F. Donatini, G. Rey, S. Siebentritt, A. Walsh, and G. Dennler, Adv. Energy Mater. 6, 1502276 (2016).
12. A. Luque, and S. Hegedus, *Handbook of Photovoltaic Science and Engineering*, 2nd edn. John Wiley and Sons, Ltd, 2011, p 1–1106.
13. T.J. Huang, X. Yin, G. Qi, and H. Gong, T.J. Huang, X. Yin, G. Qi, and H. Gong, *Phys. Status Solidi-R*, 2014, **8**, p 735.
14. S.N. Hood, A. Walsh, C. Persson, K. Iordanidou, D. Huang, M. Kumar, Z. Jehl, M. Courel, J. Lauwaert, and S. Lee, S.N. Hood, A. Walsh, C. Persson, K. Iordanidou, D. Huang, M. Kumar, Z. Jehl, M. Courel, J. Lauwaert, and S. Lee, *J. Phys. Energy*, 2019, **1**, p 042004.
15. S. Chen, A. Walsh, X.G. Gong, and S.-H. Wei, S. Chen, A. Walsh, X.G. Gong, and S.-H. Wei, *Adv. Mater.*, 2013, **25**, p 1522.

16. K. Yang, J. Sim, D. Son, D. Kim, G.Y. Kim, W. Jo, S. Song, J. Kim, D. Nam, H. Cheong, and J. Kang, K. Yang, J. Sim, D. Son, D. Kim, G.Y. Kim, W. Jo, S. Song, J. Kim, D. Nam, H. Cheong, and J. Kang, *Prog. Photovoltaics*, 2015, **23**, p 1771.
17. K. SeongYeon, K. JunHo, R. Rana Tanka, K. Kang-Woo, and K. Myeung-Hoi, Curr. Appl. Phys. 18, 191 (2018).
18. B. Khadka Dhruba, K. SeongYeon, and K. JunHo, J. Phys. Chem. C 119, 12226 (2015).
19. T. Kato, N.Y. Sakai and H.K. Sugimoto, in 40th Photovoltaic Specialist Conference IEEE (2014), pp. 0844–0846.
20. J. Jong-Ok, L. Kee Doo, O. Lee Seul, S. Se-Won, L. Doh-Kwon, K. Honggon, J. Jeung-Hyun, K. Min Jae, K. BongSoo, S. Hae Jung, and K. Jin Young, ChemSusChem 7, 1073 (2014).
21. L. Fang-I, Y. Jui-Fu, W. Yu-Ling, and K. Shou-Yi, L. Fang-I, Y. Jui-Fu, W. Yu-Ling, and K. Shou-Yi, *Green Chem.*, 2017, **19**, p 795.
22. M.I. Khalil, R. Bernasconi, L. Pedrazzetti, A. Lucotti, A. Le Donne, S. Binetti, and L. Magagnina, M.I. Khalil, R. Bernasconi, L. Pedrazzetti, A. Lucotti, A. Le Donne, S. Binetti, and L. Magagnina, *J. Electrochem. Soc.*, 2017, **164**, p D302.
23. O.K. Simya, B. Geetha Priyadarshini, K. Balachander, and A.M. Ashok, Mater. Res. Express 7, 016419 (2020).
24. Y.S. Lee, T. Gershon, O. Gunawan, T.K. Todorov, T. Gokmen, Y. Virgus, and S. Guha, Y.S. Lee, T. Gershon, O. Gunawan, T.K. Todorov, T. Gokmen, Y. Virgus, and S. Guha, *Adv. Energy Mater.*, 2015, **5**, p 1401372.
25. A. Niemegeers, M. Burgelman, K. Decock, J. Verschraegen, and S. Degrave, SCAPS manual, Version: http://scaps.elis.ugent.be/.Accessed date 19 Dec. 2016.
26. M. Patel, and A. Ray, M. Patel, and A. Ray, *Phys. B*, 2012, **407**, p 4391.
27. M. Burgelman, J. Verschraegen, S. Degrave, and P. Nollet, M. Burgelman, J. Verschraegen, S. Degrave, and P. Nollet, *Prog. Photovolt. Res. Appl.*, 2004, **12**, p 143.
28. N. Khoshsirat, and N.A.M. Yunus, in Nanoelectronics and Materials Development, ed by INTECH Open Science (2016), p. 41.
29. N. Gupta, N. Gupta, *Mater. Des.*, 2011, **32**, p 1667.
30. J.K. Grepstad, P.O. Gartland, and B.J. Slagsvold, J.K. Grepstad, P.O. Gartland, and B.J. Slagsvold, *Surf. Sci.*, 1976, **57**, p 348.
31. P.T. Moseley, P.T. Moseley, *Meas. Sci. Technol.*, 2017, **28**, p 1.
32. H. Bayad, A. El Manouni, B. Marí, Y.H. Khattak, S. Ullah, and F. Baig, H. Bayad, A. El Manouni, B. Marí, Y.H. Khattak, S. Ullah, and F. Baig, *Opt. Quantum Electron.*, 2018, **50**, p 259.
33. O.K. Simya, A. Mahaboobbatcha, and K. Balachander, O.K. Simya, A. Mahaboobbatcha, and K. Balachander, *Superlattices Microst.*, 2015, **82**, p 248.
34. L. Heng-Rui, C. Shiyou, Z. Ying-Teng, H.J. Xiang, X.G. Gong, and W. Su-Huai, L. Heng-Rui, C. Shiyou, Z. Ying-Teng, H.J. Xiang, X.G. Gong, and W. Su-Huai, *J. Appl. Phys.*, 2012, **112**, p 093717.
35. W. Shockley, and W.T. Read, W. Shockley, and W.T. Read, *Phys. Rev.*, 1952, **87**, p 835.
36. G.K. Paul, R. Ghosh, S.K. Bera, S. Bandyopadhyay, T. Sakurai, and K. Akimoto, G.K. Paul, R. Ghosh, S.K. Bera, S. Bandyopadhyay, T. Sakurai, and K. Akimoto, *Chem. Phys. Lett.*, 2008, **463**, p 117.
37. B.L. Guo, Y.H. Chen, X.J. Liu, W.C. Liu, and A.D. Li, B.L. Guo, Y.H. Chen, X.J. Liu, W.C. Liu, and A.D. Li, *AIP Adv.*, 2014, **4**, p 097115.
38. D.S. Murali, S. Kumar, R.J. Choudhary, A.D. Wadikar, M.K. Jain, and A. Subrahmanyam, D.S. Murali, S. Kumar, R.J. Choudhary, A.D. Wadikar, M.K. Jain, and A. Subrahmanyam, *AIP Adv.*, 2015, **5**, p 047143.
39. J.W. Hodby, T.E. Jenkins, C. Schwab, H.H. Tamurag, and D. Trivich, J.W. Hodby, T.E. Jenkins, C. Schwab, H.H. Tamurag, and D. Trivich, *J. Phys. C.*, 1976, **9**, p 1429.
40. Z. Qingwei, Z. Yihe, Z. Fengshan, L. Fengzhu, Y. Ye, F. Feidi, and P.K. Chu, Z. Qingwei, Z. Yihe, Z. Fengshan, L. Fengzhu, Y. Ye, F. Feidi, and P.K. Chu, *Chem. Eng. J.*, 2011, **171**, p 61.
41. Y. Wang, S. Lany, J. Ghanbaja, Y. Fagot-Revurat, Y.P. Chen, F. Soldera, D. Horwat, F. Mucklich, and J.F. Pierson, Y. Wang, S. Lany, J. Ghanbaja, Y. Fagot-Revurat, Y.P. Chen, F. Soldera, D. Horwat, F. Mucklich, and J.F. Pierson, *Phys. Rev. B*, 2016, **94**, p 245418.
42. T.K.S. Wong, S. Zhuk, S. Masudy-Panah, and G.K. Dalapati, T.K.S. Wong, S. Zhuk, S. Masudy-Panah, and G.K. Dalapati, *Materials*, 2016, **9**, p 271.
43. A. Niemegeers, M. Burgelman, and A. DeVos, A. Niemegeers, M. Burgelman, and A. DeVos, *Appl. Phys. Lett.*, 1995, **67**, p 843.
44. A. Redinger, M. Mousel, M.H. Wolter, N. Valle, and S. Siebentritt, A. Redinger, M. Mousel, M.H. Wolter, N. Valle, and S. Siebentritt, *Thin Solid Films*, 2013, **535**, p 291.
45. I. Repins, C. Beall, N. Vora, C. Dehart, D. Kuciauskas, P. Dippo, B. To, J. Mann, W.C. Hsu, A. Goodrich, and R. Noufi, I. Repins, C. Beall, N. Vora, C. Dehart, D. Kuciauskas, P. Dippo, B. To, J. Mann, W.C. Hsu, A. Goodrich, and R. Noufi, *Sol. Energy Mater. Sol. Cells*, 2012, **101**, p 154.
46. H. Katagiri, K. Jimbo, S. Yamada, T. Kamimura, W.S. Maw, T. Fukano, T. Ito, and T. Motohiro, H. Katagiri, K. Jimbo, S. Yamada, T. Kamimura, W.S. Maw, T. Fukano, T. Ito, and T. Motohiro, *Appl. Phys. Express*, 2008, **1**, p 041201.
47. S. Siebentritt, S. Siebentritt, *Thin Solid Films*, 2013, **535**, p 1.